Tolerance-Resolved Cascade Calibration of a Silicon Air-Microfluidic Virtual Impactor for Compact PM_{10} and $PM_{2.5}$ Sampling

Dr. Rafay Tallat[1,*] and Dr. Naresh Chandra[1]

[1] Indian Institute of Technology Delhi, Hauz Khas, New Delhi-110016
* Correspondence: rafya.tal@iitd.ac.in

Abstract: A practical air quality instrument needs a separator that will provide a consistent aerodynamic fraction of particles to the sensor element, rather than an unconstrained combination of coarse and fine particles. This paper presents an inquiry into the nature of a dual-stage silicon microfluidic virtual impactor as a practically manufacturable $PM_{10}/PM_{2.5}$ cascade based on geometrical parameters, manufacturing tolerance, simulated collection efficiency, and particle monodispersity measurements. In this particular case, the separator comprises a coarse stage with $W_1/D_1/S_1/M_1/\phi_1 = 450/200/640/700/75$ and a fine stage with $W_2/D_2/S_2/M_2/\phi_2 = 250/200/280/300/75$, with linear dimensions specified in micrometers and angular measurements in degrees. The simulation takes into account air density 1.29 kg m^{-3}, dynamic viscosity 1.81×10^{-5} Pa s, maximum allowable deviation in silicon-on-insulator manufacturing process 10 µm, nine monodisperse aerosols from 1.5 µm to 15 µm, and actual testing with a TSI 6301 counter running at 2.83 L min^{-1}. Simulated cutoff diameters are found to be 2.55 µm for fine and 9.90 µm for coarse stages, using linear interpolation and logistic function reconstruction. While having more gradual transition, the fine stage has a sharper cutpoint at a local gradient of 0.253 μm^{-1}, with the measured points pushing the transition point toward 3.56 µm to 3.79 µm. Coarse stage remains efficient above 50% threshold across all available monodispersive particle sizes, thus failing to completely determine its measured transition point. The primary observation is that cascade efficiency is determined not by the presence of the two cut points but rather by the fine-stage tolerance and stability of flow rate at the end of the cascade. Large channel width and feed flow rate have the largest influence on performance, small channel width influences mostly deposition, 75° branch angle determines the optimal compromise between trajectory separation and wall impact, and channel length primarily acts as a packaging parameter. The analysis provides a complete stage-resolved interpretation of a compact PM separator for portable air-monitoring modules.

Keywords: virtual impactor; PM_{10}; $PM_{2.5}$; microfluidic separator; MEMS fabrication; cutpoint fidelity; collection efficiency; aerosol sampling; wall loss; portable air-quality sensor

Citation: Dr. Rafay Tallat and Dr. Naresh Chandra. 2022. Tolerance-Resolved Cascade Calibration of a Silicon Air-Microfluidic Virtual Impactor for Compact PM_{10} and $PM_{2.5}$ Sampling. *TK Techforum Journal (ThyssenKrupp Techforum)* 2022(2): 62–78.

Received: May-20-2022
Accepted: September-22-2022
Published: September-30-2022

1. Introduction

Precise measurements of particulate matter start before any particles enter the detection mechanism. Optical scattering sensors, quartz crystal microbalances, resonant MEMS structures, surface acoustic waves, and electrical particle counters all rely on the size distribution of aerosols entering the sensing volume. In other words, the naming of the PM_{10} and $PM_{2.5}$ fractions is not simply descriptive; there is an intrinsic requirement for an aerosol sampling inlet that separates particles based on inertia and flow following ability. While it is possible to construct a stable electrical or optical detection scheme, the measurement of aerosol concentrations by such sensors alone lacks interpretability in terms of the particular fraction relevant to human health [1–4].

It has become increasingly important to reduce the physical footprint of sampling inlets for the reasons outlined above. Air quality monitoring has shifted away from static

installations to more distributed and mobile instruments with denser spatial sampling. At the same time, sensitivity to variations in humidity, refractive index, aerosol composition, aerosol morphology, and inlet losses is typical of many miniaturized aerosol sampling systems [5–8]. The sampler becomes an integral part of the measurement process rather than a simple inlet. Factors like the position of the cutpoint, the slope of the cutpoint, the degree of wall loss, flow dependencies, and the potential for manufacturing dictate whether an inlet will allow for comparison of the output signal to regulatory PM classes or mechanistic studies of aerosol exposure.

Virtual impactors can play an important role in these applications due to the inertial mismatch between aerosol particles and gas flow in absence of complete collection of the target fraction onto a solid wall. Larger particles follow the turning gas flow towards the minor flow direction where they exit the separator along with the minor flow, whereas smaller particles follow the major gas flow direction. Virtual impaction technology has been developed for decades, finding application in dichotomous samplers, clean air core impactors, highly efficient virtual impactors, and slit nozzle virtual impaction systems [9–19]. There are clear physical underpinnings of this approach, but they also demonstrate that there is more involved in the process of aerosol sampling than merely inertial effects of the particles. The nozzle width, receiver spacing, fraction of minor flow, branch angle, and velocity have to work together in order for the desired particle size to enter the intended exit.

Miniaturization exacerbates the design issues at play. Changes in size on the scale of micrometers affect local velocity, streamline curvature, alignment with the receiver, and the stopping distance in relation to the width of the air channel. Examples of virtual impactor-integrated sensing modules in air-microfluidics include personal monitors, MEMS deposition sensors, SAW, QCM, and portable grading chips [20–26]. These devices exploit their small volume, small sample holdup, and suitability for mass production; however, they have poor dimensional tolerance for changes in design features. What is a small change in dimension in a traditional particle sampler may well translate into a substantial relative change in the dimensions of a microchannel.

The recent literature on air-microfluidic separators and MEMS has pointed out the dependence of aerosol separation performance on the interplay of geometrical parameters and fluid flow [27–35]. It is not just whether the expected separation of particle populations will occur at all, but rather whether the predictions hold up in actual design and manufacture of a working device. The question becomes even more complex in the case of a two-stage separator where the output of the first stage feeds the input of the second stage, whose efficiency is crucial to generating the PM population of interest.

This paper considers a particular example of a two-stage air-microfluidic separator consisting of silicon-based microfabrication components with a virtual impactor configuration capable of classifying particles of a PM_{10} stream into PM_{10} and $PM_{2.5}$ [36]. In effect, the design consists of a coarse stage followed by a fine stage, producing three streams: a PM_{10}-dominated coarse stream, an intermediate $PM_{2.5}$–PM_{10} stream, and a fine $PM_{2.5}$ stream. This raises the question about what geometry and design variable in a two-stage separator define its $PM_{10}/PM_{2.5}$ identity.

The solution is achieved using stage-specific calibration rather than with a generic analysis of virtual impactors. Efficiency points are constructed from simulated points to get cutpoint and slope data. Measurement points acquired via tests using monodisperse particle standards are correlated to determine whether the actual separator retains the simulated transition. Manufacturing tolerances are mapped as fractional dimensional uncertainty in order to allow interpretation of the same 10 µm tolerance value differently in each stage. In effect, geometric-flow behavior is treated as a control hierarchy. Such a structure ensures focus within the document itself on the particular separator being considered, prevents the mixing up of the stages, and ties the numerics explicitly to practical PM-sensor applications.

2. Device basis and measurement record

The separator is a two-stage microfluidic system built with silicon-on-insulator substrate technology. The first virtual impactor acts upon the inlet aerosol to perform the upper separation around the PM_{10} cutoff. The minor branch carries off the coarse fraction, while the rest flows onward to the second virtual impactor. The second stage performs the lower separation around the $PM_{2.5}$ cutoff, delivering both an intermediate outlet for particles from the fine class and the major flow outlet for particles in the fine fraction. This cascading configuration makes a difference since the second stage encounters aerosols different from those at the inlet due to the coarse classification at the first stage.

The values used in Table 1 are necessary in order to determine the physical environment of the chip. First of all, density and viscosity are required since the operation of the virtual impactor depends on whether or not a particle is capable of retaining its trajectory in the curved gas stream. The dimensional deviation parameter is also important. For example, a deviation of 10 µm means very little compared to the width of the first-stage receiver but more compared to the nozzle and spacing sizes of the second stage. Flow rate is included as an intrinsic property of the design because an otherwise identical geometry run at a different flow will have a different cutpoint.

Table 1. Physical inputs.

Quantity	Value	Role in analysis
Air density ρ	1.29 kg m^{-3}	Particle-gas inertia relation
Dynamic viscosity μ	1.81×10^{-5} Pa s	Stokes drag and cutpoint scaling
Maximum dimensional deviation	≤ 10 µm	Fabrication-tolerance audit
Counter flow rate	2.83 L min^{-1}	Measured outlet counting condition
Particle-diameter span	1.5 µm to 15 µm	Measurement support for both cut regions

The configuration presented in Figure 1 makes clear the cascading nature of the device; it is not a combination of two devices put one after another. This is because the upstream branch extracts a coarse-rich flow before reaching the second stage. As a result, it is the downstream fine stage that classifies the final $PM_{2.5}$ particles, however its input is affected by what happened upstream. Any attempt to average out both stages will miss the connection between them.

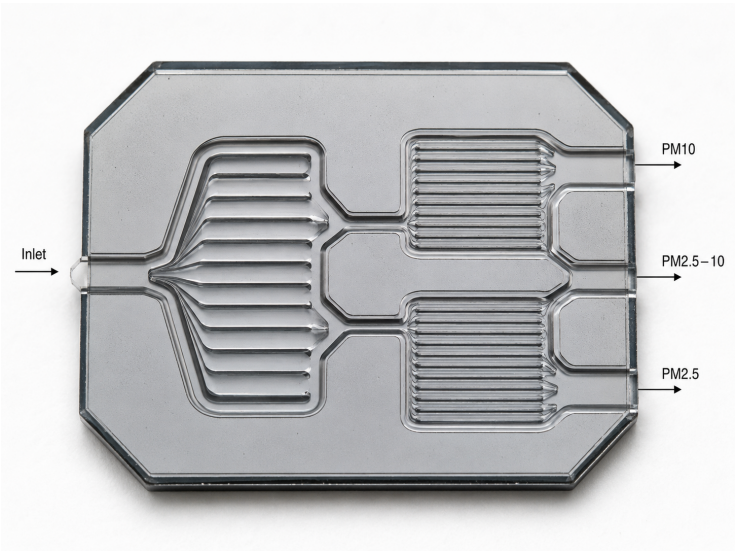

Figure 1. Two-stage separator.

The roles in Table 2 show that the measured performance of the final outlet depends most strongly on the downstream virtual impactor. The first stage must keep coarse particles from overwhelming the downstream classification, but the $PM_{2.5}$ meaning of the final

stream is assigned by the second stage. This distinction underlies the later interpretation that the fine stage is the critical stage for functional accuracy even when both simulated cutpoints appear close to the desired PM thresholds.

Table 2. Stage functions.

Circuit element	Intended aerodynamic role	Outlet interpretation
Stage 1 virtual impactor	Coarse decision around the PM_{10} range	Minor outlet enriched in particles above the coarse threshold
Interstage stream	Aerosol passed after coarse removal	Feed for the fine decision stage
Stage 2 virtual impactor	Fine decision around the $PM_{2.5}$ range	Final fine outlet and intermediate $PM_{2.5}$–PM_{10} stream

First, the difference in dimensions seen in Table 3 suggests that the tolerance risk should be applied differently to the two stages. Note that the major and minor widths of the fine stage are substantially lower than those in the coarse stage. As the particle classification process is determined by the ratio between inertia stoppage behavior and gas curvature at the channel scale, any given error will be more pronounced aerodynamically for the fine stage. Although the common branch angle of 75° means that both stages have been designed under similar receiver angles philosophy, the difference in geometries places them into different sensitivity regions.

Table 3. Stage geometry.

Stage	W (μm)	D (μm)	S (μm)	M (μm)	ϕ (°)
Coarse stage	450	200	640	700	75
Fine stage	250	200	280	300	75

Figure 2 illustrates a physical understanding of the two outlet choices. Bigger particles continue their rectilinear motion when the flow deviates from its path and hence are sorted towards the coarse-rich branch. Smaller particles tend to follow the curvilinear path defined by the fine stage outlets and are chosen by the second virtual impactor. It is important to note that the separator is an inertial classifier and thus should not be viewed as a filter with a single-pore size.

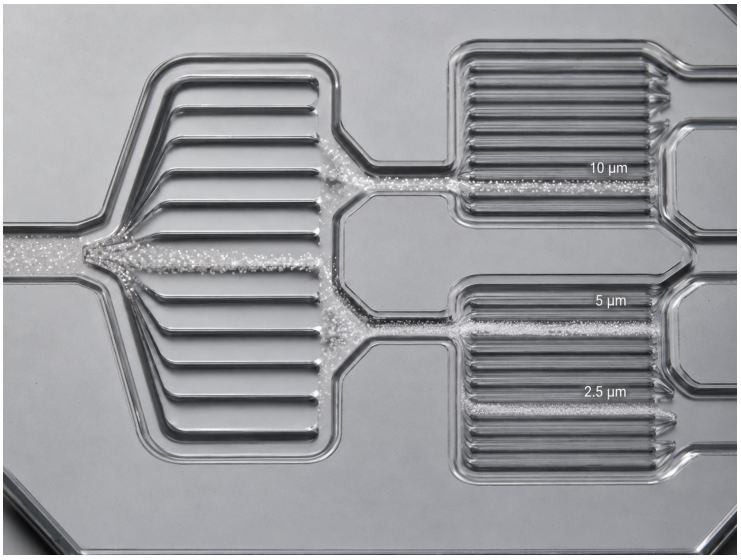

Figure 2. Particle-path selection.

The metrology perspective illustrated in Figure 3 illustrates that the nominal drawing is related to the operating separator through their shared process deviation occupying different percentages of the active channel widths. The use of silicon-on-insulator technology provides excellent dimensional repeatability, and the deviation value of not greater than 10 µm provides good manufacturing results. However, the aerodynamic significance of the

deviation can be considered only in terms of its location. If one considers a deviation value of 10 µm, it becomes 2.2 % of the width of the first stage (W_1) but 4.0 % of the second stage (W_2); and approximately 1.6 % of S_1, but 3.6 % of S_2. These fractional differences justify treating fabrication tolerance as a performance variable rather than as a simple process note.

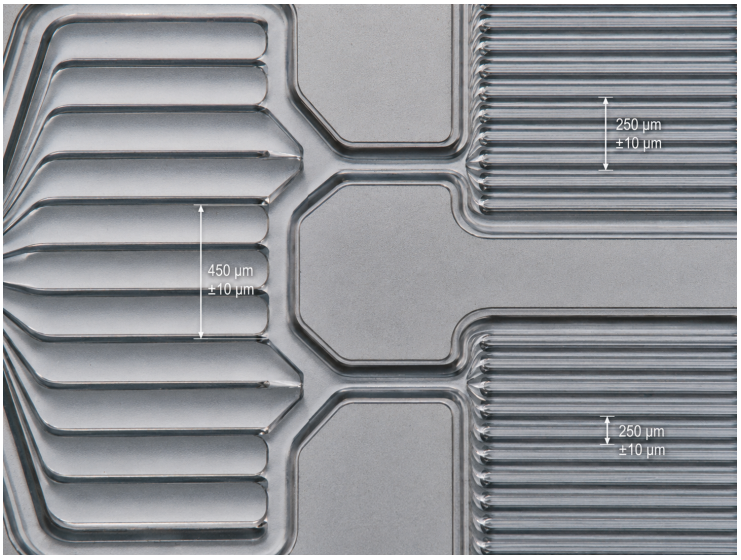

Figure 3. Dimensional metrology.

The standard-particle set in Table 4 is well positioned for the $PM_{2.5}$ neighborhood because it includes 2.0 µm, 2.5 µm, and 3.0 µm particles. This density of particle sizes makes the fine-stage displacement visible. The coarse region is less tightly sampled. Particles of 9.0 µm, 10.0 µm, and 15.0 µm place the first-stage response in the correct aerodynamic range, yet the gap between 10.0 µm and 15.0 µm limits the precision with which a measured coarse d_{50} can be located.

Table 4. Particle standards.

Standard	Diameter (μm)	Dosage (g)	Particle count
S1	1.5	0.20	5.38×10^9
S2	2.0	0.20	2.27×10^9
S3	2.5	0.20	1.16×10^9
S4	3.0	0.30	6.74×10^8
S5	5.0	0.20	1.45×10^8
S6	7.0	0.10	5.30×10^8
S7	9.0	0.14	2.49×10^8
S8	10.0	0.20	1.82×10^8
S9	15.0	0.30	5.39×10^7

The measurement chain illustrated in Figure 4 suggests that the reported efficiencies are system-level properties. Aerosol generation in a 10 L gas bag, chip transfer, aerosol collection at the outlet, and subsequent counting with the TSI 6301 at 2.83 L min^{-1} all play a role in the recorded efficiency. This fact needs to be taken into account in the analysis. In fact, a discrepancy between a theoretical prediction and a measurement cannot always be attributed to a single parameter. It might be related to size distribution, flow pattern, particle generation, wall interaction, counting error, or some combination thereof.

One must bear in mind the context of the measurement data. The maximum count rate is observed at the minimum particle size, and the number of available particles is very low beyond the 15 µm standard. This distribution is typical of practical aerosol experiments, as it is easier to aerosolize smaller particles than larger ones. It implies that the fine-stage

measurement benefits from a dense and particle-laden series of standards, whereas the coarse-stage measurement relies heavily on a few large-diameter particle checks. This situation is clearly not balanced between the two cutpoints, and it needs to be reflected in the reliability of the corresponding measured transitions.

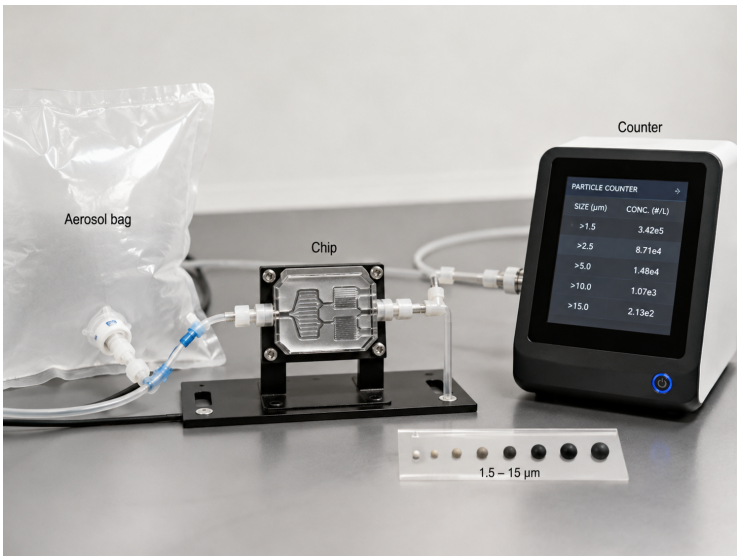

Figure 4. Measurement setup.

The basis of the device explains why it is relevant for compact aerosol sensing and not just for aerosol sampling in the lab. A microfabricated cascade of channels can be positioned immediately upstream of a detector, minimizing the volume of aerosol in transit and thus eliminating the uncertainty that stems from measuring the aerosol in a pipe after classifying it. While such placement was an attractive design principle behind many MEMS-based aerosol instruments, it is of use only if the transfer function of the aerosolizer is well characterized [37]. This particular geometry thus needs to be evaluated as a combined separator-detector unit: the aerosol classification must be sufficiently precise to enable a meaningful measurement by the downstream detector.

3. Reconstruction of the performance of the cascade separator

Inertial separation in terms of a Stokes number definition is the starting point of the physical discussion. For a particle with a diameter d_p entering a characteristic channel of width W_c and gas velocity U, the corresponding dimensionless value may be expressed as

$$\mathrm{Stk} = \frac{\rho_p C_c d_p^2 U}{9\mu W_c}, \tag{1}$$

where ρ_p is the particle density, C_c is the slip correction factor, and μ is the gas dynamic viscosity [1,2,9]. The formula describes the fundamental tradeoff between the parameters of a micro-virtual impactor. Smaller channel size and larger velocity improve particle inertial discrimination but increase the likelihood that a particle will collide with the wall.

Stage collection efficiency is considered a function of the outlet probability with respect to diameter. In general, the response for stage i can be formulated as follows:

$$\eta_i(d) = \frac{N_{i,\mathrm{classified}}(d)}{N_{i,\mathrm{in}}(d)}, \tag{2}$$

where $\mathrm{N}_{i,\mathrm{classified}}$ represents the count belonging to the classified output stream, while $\mathrm{N}_{i,\mathrm{in}}$ is the number of particles incoming into the stage. The reason why such definition is adopted lies both in the fact that the available evidence is provided in terms of stagewise

efficiency points only, and the decision of avoiding any assumption about the combined inlet process performed by both stages.

Cutpoint estimation with linear interpolation is performed for pairs of neighboring points (d_a, η_a) and (d_b, η_b) that bracket $\eta = 0.5$. The cutpoint of interest is calculated as follows:

$$d_{50,\mathrm{lin}} = d_a + \frac{0.5 - \eta_a}{\eta_b - \eta_a}(d_b - d_a). \tag{3}$$

The resulting value allows a straightforward reading of a possible cutpoint from the points table; however, the lack of an underlying assumption about curve shape becomes both a merit and drawback since no valid estimation of cutpoint is produced if the measurements do not bracket 50

A logistic function is chosen to represent a smooth response function:

$$\eta(d) = \eta_L + \frac{\eta_U - \eta_L}{1 + \exp\{k(d - d_{50})\}}, \tag{4}$$

where η_U and η_L stand for limiting values of efficiency, and k controls the sharpness of transition. Note that the choice of such representation does not imply any new model assumptions for particle transport processes. Instead, it is used solely as a tool to interpolate stagewise points and measure transition characteristics.

The local transition sharpness is evaluated as

$$S_{50} = \left| \frac{d\eta}{dd} \right|_{d=d_{50}}. \tag{5}$$

A large value of S_{50} indicates that fewer particle diameters occupy the ambiguous part of the curve. This quantity is especially important for a cascade because an apparently well-centered cutpoint may still perform poorly if the transition is too gradual. Conversely, a sharp simulated transition may be operationally fragile if a small dimensional or flow perturbation moves it away from the desired PM boundary.

Simulation-measurement agreement is summarized by the mean absolute error and root-mean-square error,

$$\mathrm{MAE} = \frac{1}{n}\sum_{j=1}^{n} \left| \eta_{\mathrm{meas},j} - \eta_{\mathrm{sim}}(d_j) \right|, \tag{6}$$

$$\mathrm{RMSE} = \left[\frac{1}{n}\sum_{j=1}^{n} \{\eta_{\mathrm{meas},j} - \eta_{\mathrm{sim}}(d_j)\}^2 \right]^{1/2}. \tag{7}$$

These values are interpreted as stagewise diagnostic quantities rather than as universal pass-fail scores. A small error can still be incomplete if the measured points do not bracket the cutpoint. A larger error near $\mathrm{PM}_{2.5}$ may be more consequential than a comparable error far from a regulatory or health-relevant boundary.

Fabrication tolerance is expressed as a fractional deviation,

$$\tau_x = \frac{\Delta x_{\max}}{x}, \tag{8}$$

where $\Delta x_{\max} = 10\,\mu\mathrm{m}$ and x is a nominal channel dimension. This conversion is needed because tolerance has no single aerodynamic meaning in a multi-scale cascade. The same process deviation represents 5.0 % of the 200 µm depth but only 1.4 % of the 700 µm first-stage minor width. The downstream stage is therefore expected to be more vulnerable to dimensional drift, especially through W_2, S_2, and M_2.

The reconstruction procedure follows the physical order of the device. Stagewise simulated points are first converted into linear and logistic cutpoints. Measured points are then compared against the corresponding simulated trends. The geometry-flow variables are finally interpreted in relation to cutpoint movement, transition sharpness, and wall loss.

This order keeps the analysis tied to the cascade: geometric design creates the predicted transition, fabrication tolerance modifies the realized geometry, and measurement reveals how the operating device expresses that geometry under particle loading and flow.

The method also preserves a distinction between interpolation and extrapolation. A cutpoint bracketed by measured or simulated points is treated as a local result because it lies inside the observed diameter interval. A transition estimated outside the available measured points is treated only as a tendency. This distinction is essential for the coarse stage, where the measured values remain above 50% through 9.899 µm. The numerical extrapolation can suggest where the crossing may lie, but it cannot replace direct particle-standard evidence in the PM_{10} region.

Another reason for using both linear and logistic reconstructions is that they answer different questions. The linear value answers the immediate engineering question of where the two neighboring points cross the 50% threshold. The logistic curve gives a smoothed interpretation of the whole available response and permits a slope estimate. Agreement between the two estimates increases confidence in the cutpoint, while disagreement would indicate that the transition is either poorly sampled or not well represented by a single smooth curve. In the present separator, the close agreement for the fine stage supports a robust simulated $PM_{2.5}$ cutpoint, whereas the measurement comparison reveals that the operating device shifts away from that ideal.

4. Performance assessment

4.1. Location and sharpness of the two separation windows

The simulated response in Table 5 places the fine-stage transition almost directly at the $PM_{2.5}$ threshold. The value at 2.516 µm is 0.509, which means that a small interpolation interval is sufficient to locate the fine d_{50}. The coarse stage is centered near PM_{10} but changes more gradually. Its response remains 0.571 at 9.009 µm and falls to 0.370 by 11.529 µm. The two stages therefore do not have identical response shapes. The downstream fine stage is closer to a sharp classifier, while the upstream coarse stage behaves as a broader preseparator.

Table 5. Simulated response.

Fine stage			Coarse stage		
d (μm)	η	Response zone	d (μm)	η	Response zone
0.503	0.759	plateau	6.016	0.757	high-efficiency side
1.007	0.755	plateau	7.069	0.721	high-efficiency side
2.516	0.509	cut region	8.007	0.665	upper approach
3.520	0.255	falling branch	9.009	0.571	cut approach
4.507	0.139	lower branch	11.529	0.370	post-cut side
6.016	0.090	lower tail	13.520	0.336	lower tail

Table 6. Cutpoint estimates.

Quantity	Fine stage	Coarse stage
Linear d_{50} (μm)	2.552	9.899
Logistic d_{50} (μm)	2.547	9.656
Approximate d_{16} from logistic fit (μm)	4.250	not bracketed
Local slope at d_{50}, S_{50} (μm^{-1})	0.253	0.080
Logistic-fit RMSE	8.63×10^{-4}	3.50×10^{-3}

The values in Table 6 support two conclusions. The linear and logistic d_{50} estimates are nearly identical for the fine stage and close for the coarse stage, so the main cutpoint locations are not artifacts of the reconstruction method. The slope values, however, differ strongly. The fine-stage slope is more than three times the coarse-stage slope, which means that the fine stage gives a tighter transition around its nominal threshold. This tighter

transition is useful for $PM_{2.5}$ discrimination, but it also makes a displacement of the fine-stage curve more consequential because a small shift can move a substantial part of the near-threshold particle population to the wrong outlet.

This separation is evident from the Figure 5 as the fine-stage curve falls steeply in the area between 2.5 µm and 4.0 µm, while the coarse-stage curve remains high all the way into the PM_{10} region. This difference in transition zone positions is the key aerodynamic characteristic of the design, since it allows for creation of the coarse, intermediate, and fine streams. If these transition zones were too close, no clear distinction between the streams could be achieved; similarly, the curves would have to be narrowly spaced to minimize overlap of outlet fractions. The current set of curves, therefore, suggests that a two-stage virtual impactor design is preferable to a one-stage compromise design.

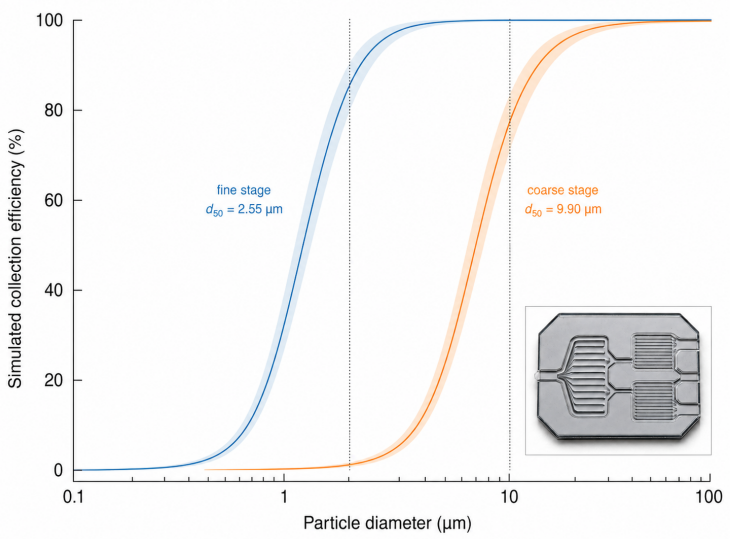

Figure 5. Simulated cutpoints.

The fine-stage curve, in turn, is positioned with the purpose of distinguishing between particles close to the 2.5 µm threshold. As discussed earlier, the number of particles in that region is significant in many aerosols, especially urban. Therefore, any errors in the $PM_{2.5}$ cut will be highly consequential. An upward shift in the position of the fine-stage transition line results in the reclassification of the particles in the question, thus having a critical effect on the $PM_{2.5}$ performance. In contrast, the coarse stage does not contribute directly to the final classification; a possible moderate uncertainty in the coarse slope would be limited only to the intermediate stream. Therefore, the highest priority should be given to the second virtual impactor.

The coarse stage, being a preliminary filter, does not need to produce accurate size cut-offs; instead, the task is to reduce particle load for the downstream classifier. Consequently, the transition zone of the coarse stage curve is wider, which means that the transition itself is more uncertain. However, since the purpose of the first stage is to ensure proper operation of the downstream fine classifier by filtering out the largest particles, there may be no issues associated with this type of error. In fact, it may be reasonable to use a coarse transition centered near the PM_{10} region as long as the intermediate outlet is treated properly.

4.2. Measured alignment of the operating cascade

The measured response in Table 7 identifies a difference between simulated and operating behavior. The fine-stage value at 2.727 µm is 0.629, higher than would be expected if the simulated transition centered exactly at 2.55 µm under the same conditions. The value at 5.253 µm falls to 0.321, so the measured fine response does cross the transition region, but at a coarser effective diameter. The coarse-stage points remain above 0.5 through 9.899 µm, preventing a direct bracketing of the measured coarse cutpoint.

Table 7. Measured response.

Fine stage			Coarse stage		
d (μm)	η_{meas}	Position	d (μm)	η_{meas}	Position
0.707	0.789	fine side	7.020	0.789	high-efficiency side
2.727	0.629	transition side	8.939	0.689	upper approach
5.253	0.321	lower side	9.899	0.622	still above 50%

The results provided in Table 8 confirm the importance of the fine stage for proper calibration. Namely, the measured transition point is found to be about 3.56 µm to 3.79 µm. This value corresponds to an 1 µm shift compared with the simulated cut-point, which is significant in terms of $PM_{2.5}$ threshold and will affect near-threshold particle detection in a miniature sensor. At the same time, the coarse stage errors appear to be smaller, but they are not less worrying as the measured points remain above 50% throughout. Hence, the coarse channel responds consistently with PM_{10} classification, but still, it cannot provide exact resolution at the transition.

Table 8. Agreement measures.

Diagnostic quantity	Fine stage	Coarse stage
Measured linear transition diameter (μm)	3.785	not bracketed
Measured logistic transition diameter (μm)	3.557	11.687[†]
MAE relative to reconstructed simulated trend	0.137	0.100
RMSE relative to reconstructed simulated trend	0.157	0.103
Interpretation	upward fine-stage displacement	measured $d_{50} > 9.899$ μm

[†]The value is an extrapolated tendency from three points and is not treated as a directly supported measured cutpoint.

As shown in Figure 6, the fine-stage transition can also be described visually by using the graph data. The measured points remain above the simulated curve through the range near $PM_{2.5}$ boundary, indicating that the device under consideration detects a fraction of particles bigger than 2.5 µm on the fine-stage high efficiency side. The shaded area within the range of 3.56 µm to 3.79 µm emphasizes the aforementioned shift. The effect is not an inconsequential graphical shift; rather, it alters the aerodynamic signature of the fine outlet, and hence it should be mentioned when the device is employed as the front end of $PM_{2.5}$.

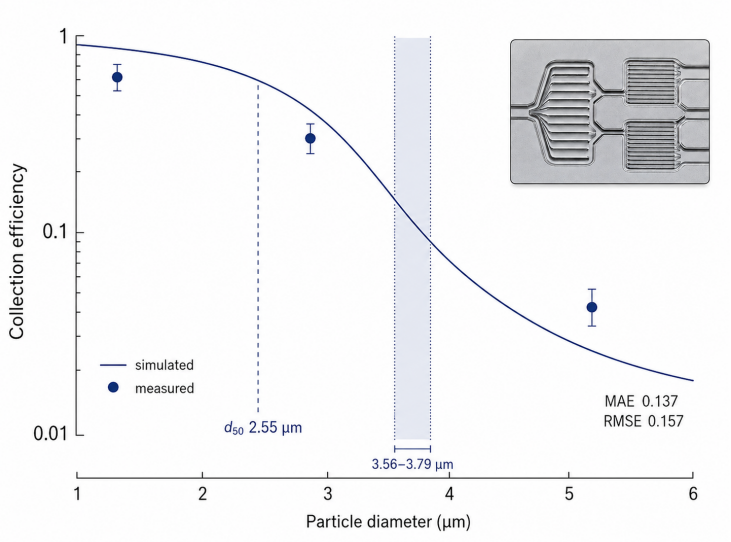

Figure 6. Fine-stage transition.

The evidence shown in Figure 7 must be understood differently than the fine stage result. While the measurements approach the 50% line and cross below it at 9.899 µm, the inference of a cross around 11.69 µm reflects only an extrapolative trend rather than fully

bracketed evidence. The distinction protects against overstating the PM_{10} validation effort. In this case, the coarse separator appears to point in the right direction, but further particles in the range 10 µm to 13 µm will confirm the measured crossing.

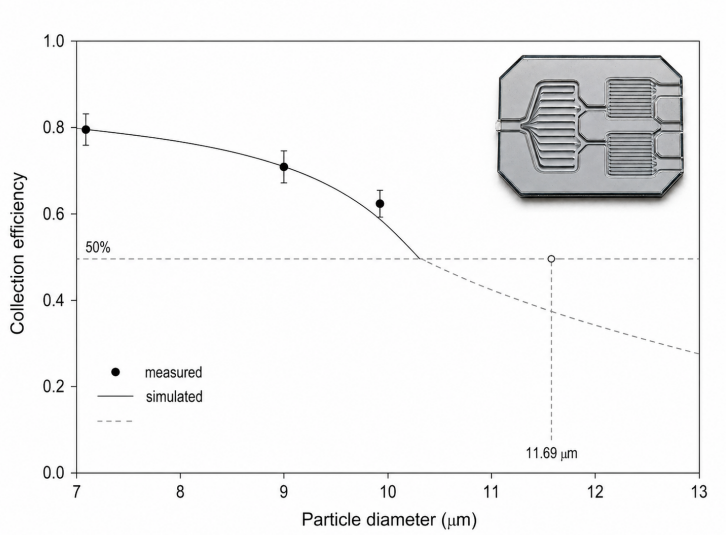

Figure 7. Coarse-stage bracketing.

An immediate benefit for future efforts can be derived from the results presented here. Future standards ought to be concentrated in regions of ambiguous evidence, such as those observed in the present case. With respect to the fine stage, standards falling within 2.5 µm to 4.0 µm could aid in determining the true displacement of the cutpoint. Similarly, standards covering 10 µm to 13 µm on the coarse stage would directly bracket the 50% crossover point. In either case, adding more evidence distant from these transition points provides fewer benefits than concentrating more points in the critical region.

A direct consequence of measuring the fine stage displacement can be identified when considering $PM_{2.5}$ monitoring. In other words, the output detector is not concerned with the cutpoint at 2.5 µm itself, but with the aerosols emitted from the working chip. When shifted upwards, the transition line implies that particles in the approximate range 2.5 µm to 4.0 µm will contribute to the final output stream more than assumed in simulation. This point is relevant due to the importance of $PM_{2.5}$ beyond its mere definition [1,4,5].

4.3. Geometry-flow priorities and wall-loss compromise

Variable effects as shown in Table 9 show why the design of the separator must follow a hierarchical design strategy as opposed to setting a standard tolerance for all variables. Major flow width and inlet flow directly modify the inertia relationship described by Eq. (1). Therefore, they exert the most direct effect on cutpoint location and curve shape. Minor flow width has more of a relation with depositional control since too much width in the receiver channel could drag trajectories into wall-impacting streams. Channel length has less of an aerodynamic effect, as classification takes place mostly around the region between nozzle and receiver.

The branch angle of 75° warrants independent analysis as well. As the angle becomes closer to the right angle at 90°, the separation becomes more abrupt, leading to more likely particle collisions with the wall as opposed to being inducted as part of the classified stream. On the other hand, a more shallow angle would reduce the likelihood of such collisions. The chosen value, however, cannot be considered purely aesthetic but a practical combination of both abrupt decision making and wall loss control.

Table 9. Control variables.

Variable	Effect on separation	Effect on wall interaction	Design consequence
Major-flow width S	Larger S weakens transition sharpness and reduces isolation of the fine boundary.	Smaller S increases wall interaction near the receiver.	Highest dimensional priority.
Minor-flow width M	Smaller influence on the cutpoint than S.	Larger M increases loss through broader turned paths.	Deposition-control dimension.
Tilt angle ϕ	A larger angle sharpens trajectory separation.	A larger angle also raises the risk of wall impact.	An angle of 75° provides a balanced receiver configuration.
Inlet flow Q	Larger Q lowers the cutpoint and steepens the separation curve.	Larger Q increases particle loss and flow sensitivity.	Highest operating priority.
Channel length L	Weak effect on the location of the separation transition.	Weak effect on particle deposition.	Secondary packaging variable.

The annotated device view shown in Figure 8 provides a manufacturing rule based on these results. The fine stage must have priority protection through controlled S_2, receiver alignment, and flow rate. The coarse stage can afford to approach the PM_{10} target more loosely because of its greater transition width. The width of the minor-flow channel should be set for optimal deposition rather than being the primary tuning variable for cutting PM_{10}. Length can be optimized in the second step after the geometry of the active part of the separator is established, assuming no unacceptable pressure drop or packaging issues.

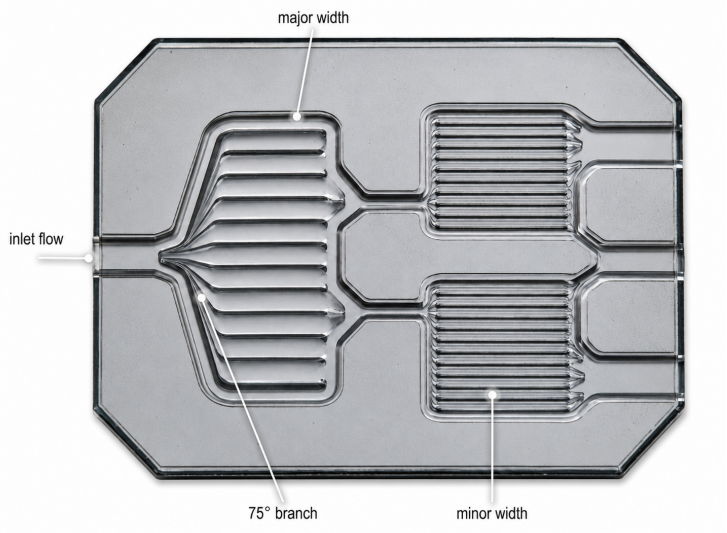

Figure 8. Geometry controls.

The actual measured displacement of the fine stage cutpoint can be explained along the same lines of hierarchical reasoning. An effective increase of S_1 in proportion to spacing, a slight reduction in local velocity, or a difference in outlet-flow split compared to the assumed simulation value would push up the fine cutpoint. As the fine stage operates with smaller sizes, the relative effects would be proportionally increased in comparison with the

coarse stage. Thus, the data reveal not only a problem to be solved but its likely locus in the space of engineering variables.

This problem would be more complicated in the case of S and Q, since both affect the same inertial criterion. Reducing channel width leads to increased average flow velocity and thus decreases the length of the near-wall turn trajectory. Similarly, increasing flow rate will make the turn sharper. These two factors have opposite effects on the cutpoint threshold: both can lower it but increase wall approach and thus deposition. This is why a separator cannot be tuned by flow alone after manufacture. Adjusting flow might compensate the shift of cutpoint threshold but would also lead to higher deposition and modified flow split.

In this context, the influence of minor-flow width becomes clear as well. By changing the way near-receiver flow joins the classified flow stream, M controls the probability of collision with the side wall for particles with intermediate velocities. As a result, M can be considered as a parameter for deposition control rather than for tuning of cutpoints. The same can be said for the classical virtual impactors: their performance depends upon the proper ratio of the secondary to inlet flows and the geometry of the receiver [38]. The present microdevice follows that older principle at a smaller length scale.

4.4. Discussion of findings

The primary research question was how effective the two-stage $PM_{10}/PM_{2.5}$ separation cascade actually was. It turns out that the cascade is characterized by two kinds of effectiveness. First, the coarse stage ensures that the upstream classification decision is made close to the PM_{10} border. Second, the fine stage classifies particles as $PM_{2.5}$, determining whether the outlet flow can be trusted in further processing. Thus, this cascade-level response is more valuable than a simple statement about the presence of two cutpoints, since it highlights what stages of the design require calibration and process control.

The predicted cutpoints seem realistic. Specifically, the fine stage's cutpoint at a diameter of about 2.55 µm is close to the lower bound for $PM_{2.5}$ definition, and the coarse stage's cutpoint near 9.90 µm coincides with the PM_{10} border. These cutpoints match the expected characteristics of an inertial cascade as well as the results of the literature on virtual impactors, according to which decreasing nozzles and increasing flow velocities lead to the shift of cutpoints downwards [10,14,27,28]. Also, the higher slope of the fine stage curve is plausible due to the tight geometry used for the fine stage forcing the transition within a narrower range of particle diameters.

The empirical results imply a slightly more nuanced conclusion. The fine stage shows a shift of the transition to a larger diameter compared to the simulation, while the coarse stage does not have measurements for the immediate vicinity of the crossing point. This result should not be considered as a flaw in the cascade's performance. Instead, it reveals the difference between a geometrically promising design and a properly calibrated PM inlet, which is crucial for creating a portable particle size sensor. The separator can support portable PM detection and classification when the realized transition is confirmed by measurements under similar flow and loading conditions.

The tolerance analysis provides further support for this conclusion. A 10 µm tolerance represents excellent fabrication in most MEMS processes, although it does not carry the same weight for all dimensions in this particular separator. At the fine stage, this tolerance equates to 4.0 % of W_2, 3.6 % of S_2, 3.3 % of M_2, and 5.0 % of D_2. All of these percentages represent significant deviations from the ideal geometry, capable of displacing the local flow field around the aerosol receiver. At the coarse stage, where dimensions tend to be larger, an equal tolerance results in a relatively minor deviation of the active geometry. The operating data provide mechanical justification for the relative importance of these tolerances as well; the fine-stage dimensions are more critical.

The second important constraint is wall loss. One could theoretically optimize towards a finer threshold by reducing the width or increasing the flow rate until the threshold is attained. However, wall loss would lead to the deposition of particulate on the channel

walls instead of allowing for classified aerosol to be delivered to the outlet port. This is the reason that virtual impactors remain attractive options for PM monitoring. The variable table and design map make it clear that S and Q are effective and dangerous controls respectively, and that M and ϕ determine how much of the separation translates into classification.

The separator serves to highlight the necessity of calibrating portable PM modules at the device level as opposed to making assumptions about component performance. Whether counting particles, employing a laser detector, or using a resonant structure to measure particle load, one expects a measurement of whatever has been sent into the instrument. In the case where the fine-stage transition has been designed too coarse, the measured value may overestimate particles exceeding the nominal $PM_{2.5}$ limit. Similarly, a loose tolerance on the coarse stage means the intermediate fraction contains more particles than intended. Calibration of portable modules is essential to account for transfer function differences between devices [5–8].

As seen in the application-oriented configuration of Figure 9, the three streams will be made available in the form of functional streams in the sensing module or the inlet collection system. The figure is illustrative since it changes the interpretation from the point of view of a chip to a deployable inlet. The portable monitor will depend on the PM_{10}, $PM_{2.5}$–PM_{10}, and $PM_{2.5}$ streams, but the nomenclature of the streams will make sense only after the verification of the transitions under the flow conditions at which the instrument operates.

Figure 9. Sensor-ready outlets.

There are several caveats about the interpretation. The sampled stagewise points have been sparsely populated, especially the coarse cutoff area. The standards have been monodisperse test particles without ambient aerosol complexity of non-uniform shape, hygroscopic behavior, and variable refractive index. The characterization has depended on efficiency points and the geometrical deviations as opposed to the three-dimensional flow fields within the chip. None of these caveats makes the conclusion invalid; it defines the extent to which the present evidence can take the matter. The device exhibits cascade performance, and its fine-stage $PM_{2.5}$ identity will be established by fine-stage calibration under the operating flow condition.

A targeted approach to the validation procedure is better than a generic approach involving the expansion of all measurements. Specifically, additional fine-stage particles of diameter 2.5 µm, 3.0 µm, 3.5 µm, and 4.0 µm will locate the upward-shifted cutpoint. Moreover, particles in the coarse stages of 10 µm to 13 µm range will establish whether the cutpoint matches the theoretical value or is above. Finally, repeated runs of the flow at

2.83 L min^{-1} will determine whether the displacement of the cutpoint results mainly from geometry or from the operation of the flow. Such a targeted approach is dictated by the data itself, and not some generic urge for more data points.

The design takeaway is that the separator needs to be specified not by the drawings, but by its cascading response in practice. For manufacturing, the fine-stage parameters must receive top priority: major width, receiver distance, and branch angles. Flow stability must be maintained during operation, since it is directly involved in the balance of the Stokes number. In reporting, the simulated and measured cutpoints should both be provided, with their brackets in terms of particle standards. Such a reporting convention will make comparison across MEMS platforms easy and make it easier to identify promising layouts from calibrated inlets.

An additional consequence of the reinterpretation is that a different standard is required for judging completeness of the manuscript. To be fully specified in this context, a manuscript must connect together the aspects of CAD geometry, fabrication parameters, estimated cut points, tolerance analysis, and operating conditions. Reporting the geometry without the particle-standard cut points leaves the realized separator uncharacterized. Reporting the measured points without the tolerance analysis leaves unexplained the increased vulnerability of the fine-stage cut point. Reporting the cut points without interpreting them in terms of wall loss overstates the classification quality. The complete description is therefore the combined one: a properly aligned cascade whose subsequent transition must be controlled and characterized since it defines the fine particle stream.

Another consequence relates to issues of reproducibility. The key information required to reproduce this result is not merely the list of dimensions, but also the mapping of dimensions onto cut point estimates. For future replication of a nominal design, the critical information is not merely the nominal dimensions, but the actual realized values of W, S, M, the branching angle, the operational flow rate, and the measured transition points. Absence of that information may hide important differences in $PM_{2.5}$ capture efficiency. This is analogous to other challenges in low-cost PM sensing, where even nominally similar devices may have substantially differing performance due to lack of characterization of inlet geometry and calibration [6–8].

Another way in which the present interpretation links this microfabricated device with the broader tradition of dichotomous particle separation is by reference to its classical antecedent. Virtual impactors were originally conceived to perform size-selective separation of aerosol streams without requiring complete collection on an impaction surface [11,12,19]. However, there is a key difference: conventional samplers can usually accommodate relatively large machining errors in relation to dimensions in millimeters, whereas MEMS designs can translate the same absolute errors into larger deviations in effective flow channel dimensions. Therefore, the current device illustrates how an existing aerodynamic principle needs to be reinterpreted in the context of microfabricated structures.

Finally, it influences how the device must be communicated to portable monitor users. Instead of simply reporting that a given instrument has a $PM_{10}/PM_{2.5}$ separator, it must also specify the fine-stage transition, the flow rate, and the particle standards used for establishing the cut region. Such information is not mere extraneous detail: it is essential for determining the comparability of $PM_{2.5}$ concentrations measured using different sensors. Indeed, as the range of portable monitoring expands, the importance of inlet characterization will become comparable to detector calibration. Only through inlet characterization can the specific aerosol reaching the detector be known [5,7,31].

5. Conclusions

Which of the stages and variables control the fidelity of this particular $PM_{10}/PM_{2.5}$ separator? The conclusions can be drawn: (a) fine stage controls the fidelity of $PM_{2.5}$ stream formation, (b) coarse stage acts as a preconditioner, and (c) simulation yields cutpoints at roughly 2.55 µm in the fine stage and roughly 9.90 µm in the coarse stage. These locations are appropriate to a PM cascade, and fine stage features a sharper transition.

Measurable evidence makes this answer more specific: (a) fine stage indicates substantial displacement in PM transition toward 3.56 µm to 3.79 µm; (b) coarse stage does not bracket PM_{10} transition; (c) efficiency remains above 50% till 9.899 µm. The separator can thus be regarded as a realistic compact cascade whose $PM_{2.5}$ fidelity needs downstream calibration and tolerance adjustment. Designing the separator for such purpose, one can identify: (a) major-flow width and inlet flow as principal variables controlling cutpoint and sharpness; (b) minor-flow width as a variable controlling deposition behavior; (c) 75° receiver angle as a compromise between separation effectiveness and wall collision probability; and (d) channel length as a subsidiary variable. Given 10 µm tolerance, the fine stage is more sensitive than the coarse stage, hence calibration and tolerance adjustments need to be performed primarily in the downstream virtual impactor. In sum, the paper finds the answer to the research question: the fine stage, major-flow width, and inlet-flow conditions determine the ability of this separator to serve reliably as a $PM_{10}/PM_{2.5}$ inlet for portable air-quality sensing.

One can conclude that the main contribution of the work in question is that the device must be considered an inlet-calibration issue, not just an advance in the field of microfabrication. The aerodynamic structure is given by geometry, but the transition determines the stream entering the sensor. Compact air-monitoring units therefore require a well-defined approach to design and testing: controlled flows, cutpoint validation, and report of PM boundary transition points.

What follows, then, is the conclusion that the separator should be approached not only as a micro-fabricated structure but also as an inlet-calibration device. It provides the desired aerodynamic configuration, but it is the transition measurement that determines the flow supplied to the detector. In the case of miniature analysis units, the proper choice is thus an airflow cascade that includes fine stage dimensions, transition measurement on the $PM_{2.5}$ edge, and documented cutpoint range. All this transforms a potentially useful separator into a reliably sampled interface.

References

[1] Hinds, W. C. Aerosol Technology: Properties, Behavior, and Measurement of Airborne Particles, 2nd ed.; Wiley: New York, NY, USA, 1999.

[2] Kulkarni, P.; Baron, P. A.; Willeke, K. Aerosol Measurement: Principles, Techniques, and Applications, 3rd ed.; Wiley: Hoboken, NJ, USA, 2011.

[3] Davidson, C. I.; Phalen, R. F.; Solomon, P. A. Airborne particulate matter and human health: A review. Aerosol Science and Technology 2005, 39, 737–749.

[4] Pope, C. A., III; Dockery, D. W. Health effects of fine particulate air pollution: Lines that connect. Journal of the Air & Waste Management Association 2006, 56, 709–742.

[5] Snyder, E. G.; Watkins, T. H.; Solomon, P. A.; Thoma, E. D.; Williams, R. W.; Hagler, G. S. W.; Shelow, D.; Hindin, D. A.; Kilaru, V. J.; Preuss, P. W. The changing paradigm of air pollution monitoring. Environmental Science & Technology 2013, 47, 11369–11377.

[6] Kumar, P.; Morawska, L.; Martani, C.; Biskos, G.; Neophytou, M.; Di Sabatino, S.; Bell, M.; Norford, L.; Britter, R. The rise of low-cost sensing for managing air pollution in cities. Environment International 2015, 75, 199–205.

[7] Morawska, L.; Thai, P. K.; Liu, X.; Asumadu-Sakyi, A.; Ayoko, G.; Bartonova, A.; Bedini, A.; Chai, F.; Christensen, B.; Dunbabin, M.; et al. Applications of low-cost sensing technologies for air quality monitoring and exposure assessment: How far have they gone? Environment International 2018, 116, 286–299.

[8] Alfano, B.; Barretta, L.; Del Giudice, A.; De Vito, S.; Di Francia, G.; Esposito, E.; Formisano, F.; Massera, E.; Miglietta, M. L.; Polichetti, T. A review of low-cost particulate matter sensors from the developers' perspectives. Sensors 2020, 20, 6819.

[9] Marple, V. A.; Willeke, K. Impactor design. Atmospheric Environment 1976, 10, 891–896.

[10] Marple, V. A.; Chien, C. M. Virtual impactors: A theoretical study. Environmental Science & Technology 1980, 14, 976–985.

[11] Masuda, H.; Hochrainer, D.; Stoeber, W. An improved virtual impactor for particle classification and generation of test aerosols with narrow size distributions. Journal of Aerosol Science 1979, 10, 275–287.

[12] Solomon, P. A.; Moyers, J. L.; Fletcher, R. A. High-volume dichotomous virtual impactor for the fractionation and collection of particles according to aerodynamic size. Aerosol Science and Technology 1983, 2, 455–464.

[13] Chen, B. T.; Yeh, H. C.; Cheng, Y. S. A novel virtual impactor: Calibration and use. Journal of Aerosol Science 1985, 16, 343–354.

[14] Chen, B. T.; Yeh, H. C. An improved virtual impactor: Design and performance. Journal of Aerosol Science 1987, 18, 203–214.

[15] Loo, B. W.; Cork, C. P. Development of high efficiency virtual impactors. Aerosol Science and Technology 1988, 9, 167–176.

[16] Chein, H.; Lundgren, D. A. A virtual impactor with clean air core for the generation of aerosols with narrow size distributions. Aerosol Science and Technology 1993, 18, 376–388.

[17] Ding, Y.; Koutrakis, P. Development of a dichotomous slit nozzle virtual impactor. Journal of Aerosol Science 2000, 31, 1421–1431.
[18] Haglund, J. S.; McFarland, A. R. A circumferential slot virtual impactor. Aerosol Science and Technology 2004, 38, 664–674.
[19] Marple, V. A. History of impactors: The first 110 years. Aerosol Science and Technology 2004, 38, 247–292.
[20] Paprotny, I.; Doering, F.; Solomon, P. A.; White, R. M.; Gundel, L. A. Microfabricated air-microfluidic sensor for personal monitoring of airborne particulate matter: Design, fabrication, and experimental results. Sensors and Actuators A: Physical 2013, 201, 506–516.
[21] Schrobenhauser, R.; Strzoda, R.; Fleischer, M.; Hartmann, A.; Amann, M. C. Detection of the mass of fine particulate matter using light scattering and inertial filtering in a miniaturized sensor setup. Measurement Science and Technology 2014, 25, 035103.
[22] Dong, M.; Iervolino, E.; Santagata, F.; Zhang, G.; Zhang, G. Integrated virtual impactor enabled PM2.5 sensor. IEEE Sensors Journal 2017, 17, 2814–2821.
[23] Kuo, F. Y.; Lin, Y. C.; Ke, L. Y.; Tsai, C. J.; Yao, D. J. Detection of particulate matter of size 2.5 μm with a surface-acoustic-wave sensor combined with a cyclone separator. Micromachines 2018, 9, 398.
[24] Wang, Y.; Wang, Y.; Liu, X.; Chen, D.; Wu, C.; Xie, J. A miniature system for separation and detection of PM based on 3-D printed virtual impactor and QCM sensor. IEEE Sensors Journal 2018, 18, 6130–6137.
[25] Fahimi, D.; Mahdavipour, O.; Sabino, J.; White, R. M.; Paprotny, I. Vertically-stacked MEMS PM2.5 sensor for wearable applications. Sensors and Actuators A: Physical 2019, 299, 111569.
[26] Poenar, D. P. Microfluidic and micromachined/MEMS devices for separation, discrimination and detection of airborne particles for pollution monitoring. Micromachines 2019, 10, 483.
[27] Chen, H. Y.; Huang, H. L. Numerical and experimental study of virtual impactor design and aerosol separation. Journal of Aerosol Science 2016, 94, 43–55.
[28] Chang, P. K.; Hsiao, T. C.; Engling, G.; Chen, J. C. Computational fluid dynamics study of the effects of flow and geometry parameters on a linear-slit virtual impactor for sampling and concentrating aerosols. Journal of Aerosol Science 2019, 131, 28–40.
[29] Chen, T.; Sun, J.; Ma, T.; Li, T.; Liu, C.; Zhu, X.; Xue, N. Design and analysis of particulate matter air-microfluidic grading chip based on MEMS. Micromachines 2019, 10, 497.
[30] Wang, P.; Yuan, S.; Yang, N.; Wang, A. Performance evaluation of a virtual impactor with an additional pretreatment structure for particle separation. Aerosol and Air Quality Research 2021, 21, 200269.
[31] Le, T. C.; Tsai, C. J.; Chang, S. Y.; Hsieh, T. H. Inertial impaction technique for the classification of aerosol particles and recent advances. KONA Powder and Particle Journal 2021, 38, 117–135.
[32] Wang, R.; Zhao, H.; Li, J.; Wang, X. Computational fluid dynamics study of the effects of temperature and geometry parameters on a virtual impactor. Micromachines 2022, 13, 1477.
[33] Wang, P.; Yuan, S.; Oppong, P. K.; Yang, N.; Wang, A. A sheathed virtual impactor–microseparator for improved separation of sub- and supercritical sized particles. Journal of Aerosol Science 2022, 164, 105999.
[34] Wang, R.; Zhao, H.; Li, J.; Wang, X. Designing a microfluidic chip driven by carbon dioxide for separation and detection of particulate matter. Micromachines 2023, 14, 183.
[35] Wang, Y.; Mei, X.; Xu, Z.; Qian, J. System integration of an optimally designed virtual impactor with a QCM sensor as a one-stop PM2.5 classification and detection platform. ACS Omega 2024, 9, 5751–5760.
[36] Li, Y.; Xu, Y.; Jiang, J.; Zhu, X.; Guo, R.; Sun, J. Design and characterization of a microfluidic circuit for air particulate matter separation. Micromachines 2022, 13, 252.
[37] Ezrre, S.; Reyna, M. A.; Anguiano, C.; Avitia, R. L.; Marquez, H. Lab-on-a-chip platforms for airborne particulate matter applications: A review of current perspectives. Biosensors 2022, 12, 191.
[38] Asgharian, B.; Godo, M. N. Transport and deposition of spherical particles and fibers in an improved virtual impactor. Aerosol Science and Technology 1997, 27, 499–506.